FIGURE 11

Fe(CO)5 Uptake Curves on H-Y

75 F and 40 psig

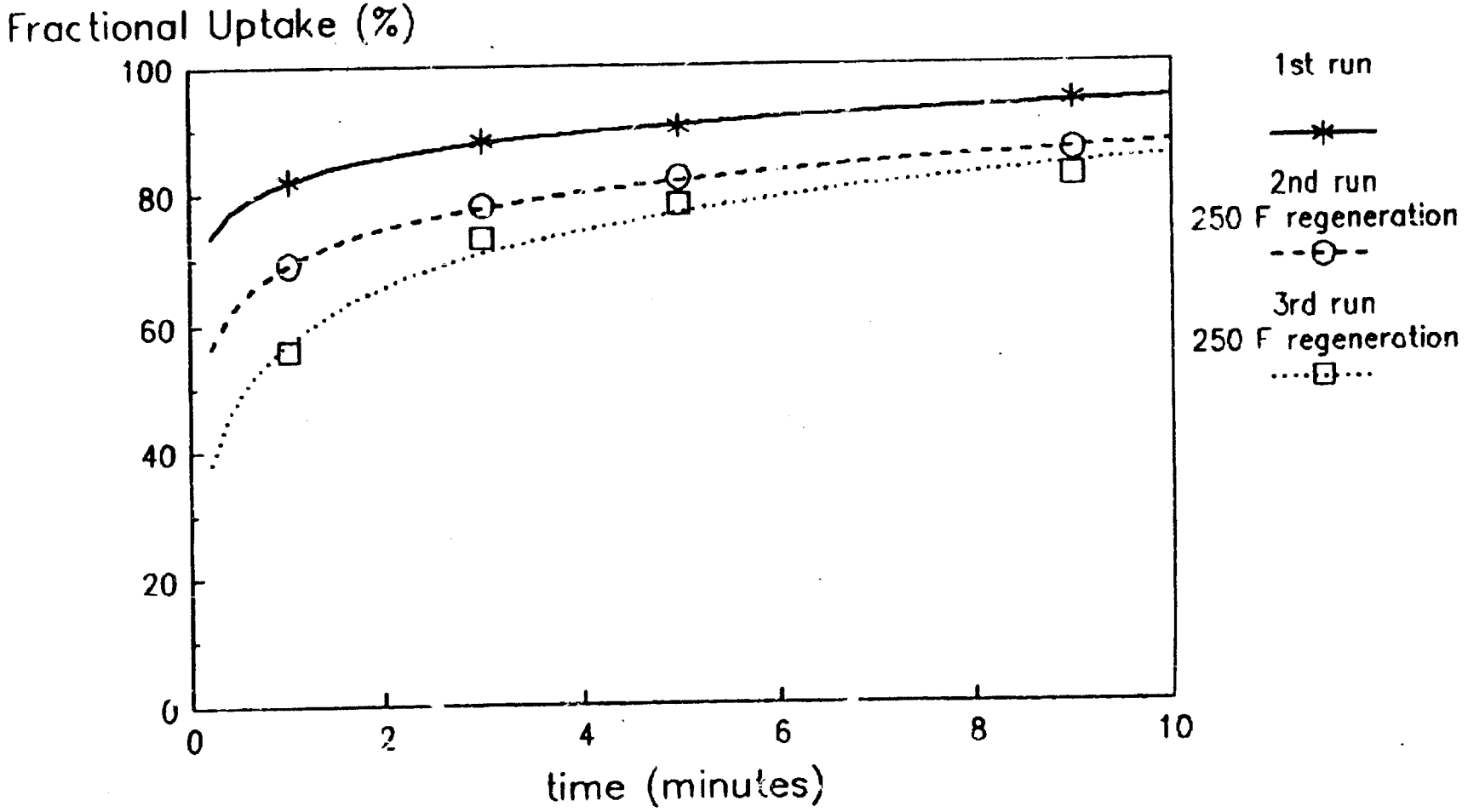

in H-Y zeolite following thermal regeneration of $Fe(CO)_5$ are larger than 12A (3). The pore size of H-Y zeolite is ~10A, therefore, it is not expected that much larger iron species are present within the zeolite structure. This suggests that the deposited iron species is outside the zeolite structure.

The thermal desorption curve of H-Y poses an interesting problem. During thermal regeneration of H-Y, the $Fe(CO)_5$ concentration in the effluent stream raises significantly. Therefore, the thermal regeneration effluent will have high concentrations of $Fe(CO)_5$ at given points. This poses an obvious safety concern. The thermal regeneration effluent is an extremely toxic off-gas that must be dealt with safely, i.e., thermal decomposition of the species may be the best practice.

In addition, a further safety concern is that thermal regeneration of $Fe(CO)_5$ laden adsorbents leads to deposition of elemental iron on the adsorbent. It is well known that supported, finely divided, metallic species are pyrophoric. Thus, when TSA beds are to be replaced, the possible pyrophoric nature of the "spent" adsorbent must be taken into consideration. This pyrophoric property is particularly a concern with respect to finely divided metallic species present on carbonaceous surfaces.

Effect of Carrier Gas Pressure on $Fe(CO)_5$ Adsorption

It is important to investigate the effect of pressure on trace impurity removal. As the pressure of the carrier gas increases, the adsorption capacity for trace impurity decreases. This is because at higher adsorption

pressures the competition for adsorption sites between the trace impurity and the bulk carrier is enhanced. Thus, the much more prevelant carrier gas molecules inhibit the adsorption of the trace impurity.

Figure 12 depicts $Fe(CO)_5$ adsorption isotherms on BPL carbon at 75°F from 40 psig (73% CO_2/26% N_2/1% CO) and 90 psig carrier (85% CO_2/14% N_2/1% CO). Clearly, the $Fe(CO)_5$ capacity is reduced when the carrier gas pressure is enhanced. At an equilibrium concentration of 5 ppm, the $Fe(CO)_5$ capacity drops from 0.96 to 0.62 mmole/g as the carrier gas pressure increases from 40 to 90 psig.

Figure 13 shows $Fe(CO)_5$ adsorption isotherms on H-Y zeolite at 75°F from 40 psig carrier (73% CO_2/26% N_2/1% CO) and 90 psig carrier (85% CO_2/14% N_2/1% CO). Once again, as in the case of adsorption on BPL, at higher carrier gas pressure, the extent of adsorption is decreased.

Mixed Langmuir Prediction of $Fe(CO)_5$ Adsorption

Since coal gasifiers operate at pressures in excess of 90 psig, it is of interest to predict adsorption capacities at higher carrier gas pressures. Prediction of multicomponent equilibrium adsorption is a difficult and complex task. Perhaps the simplest method for predicting multicomponent equilibrium adsorption is to use a mixed Langmuir approach. The working equation for the single component Langmuir isotherm is given by:

$$n = \frac{mbP}{1+bP}$$

FIGURE 12

Effect of Gas Pressure on Fe(CO)5 Adsorption

75 F, BPL Carbon

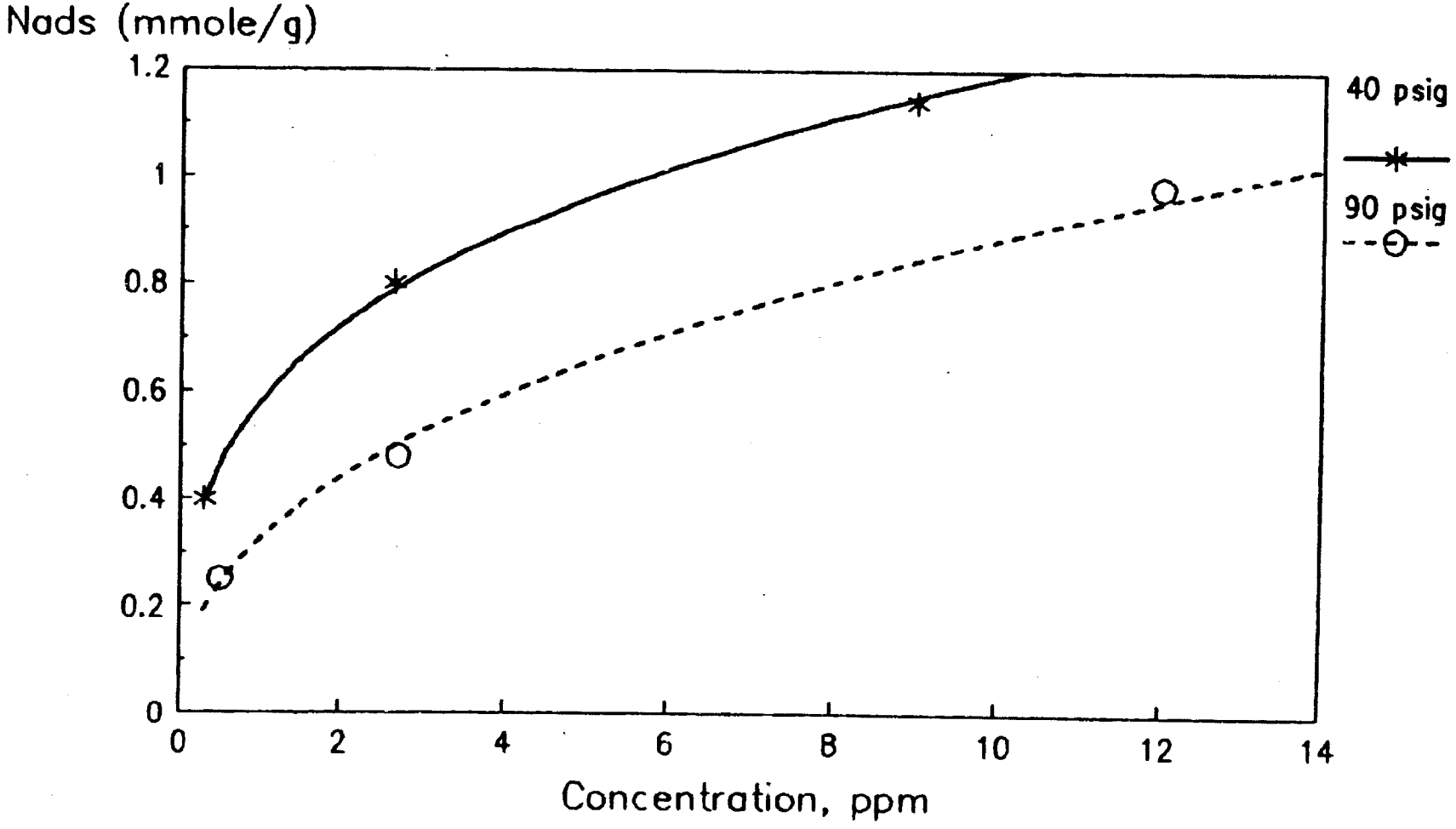

FIGURE 13

Effect of Gas Pressure on Fe(CO)5 Adsorption

75 F, H-Y

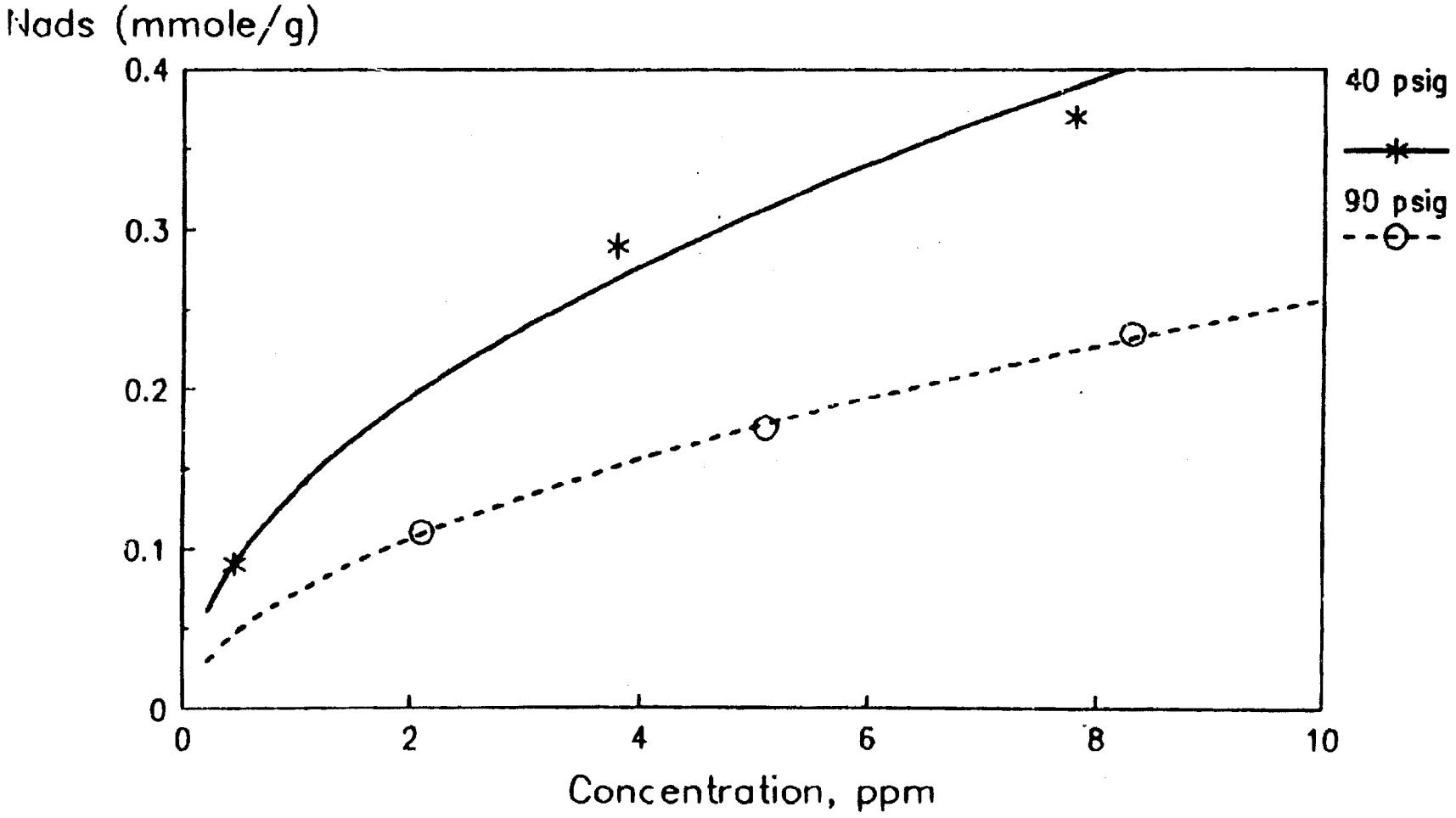

where n is the amount adsorbed, m is the monolayer capacity, b is an equilibrium adsorption coefficient, and P is the gas pressure. For the mixed Langmuir equation, the working equation is:

$$n = \frac{mbP}{1+\Sigma bP}$$

wherein the denominator of the equation is the summation of the bP products for each component in the multicomponent mixture. Thus, to predict the amount adsorbed of a given component in a multicomponent mixture one has to know a monolayer capacity, the equilibrium adsorption coefficient for each components (obtained from single component isotherms) and the partial pressure of each component in the gas mixture.

The mixed Langmuir technique was used to predict $Fe(CO)_5$ adsorption on Linde H-Y zeolite at 75°F from 90 psig carrier (85% CO_2/14% CO/1% N_2). The equilibrium adsorption coefficients for CO_2, CO, and N_2 were obtained from pure component isotherms and that for $Fe(CO)_5$ was obtained from 40 psig carrier data. Figure 14 shows the adsorption isotherms predicted by the mixed Langmuir technique and the actual experimental data. The results in Figure 14 show that the mixed Langmuir underpredicts by about 40% the amount of $Fe(CO)_5$ adsorption. At an equilibrium concentration of 5 ppm under the given conditions, the amount of $Fe(CO)_5$ adsorbed is 0.18 mmole/g vs. 0.13 mmole/g predicted by mixed Langmuir. Thus, mixed Langmuir does a reasonable job of predicting the effect of carrier gas pressure on $Fe(CO)_5$ adsorption. The theoretical value is less than the experimental value suggesting that use of the theory will provide a conservative estimate of adsorption capacity.

FIGURE 14

Mixed Langmuir Prediction of Fe(CO)5 Adsorption

75 F, 90 psig on H-Y

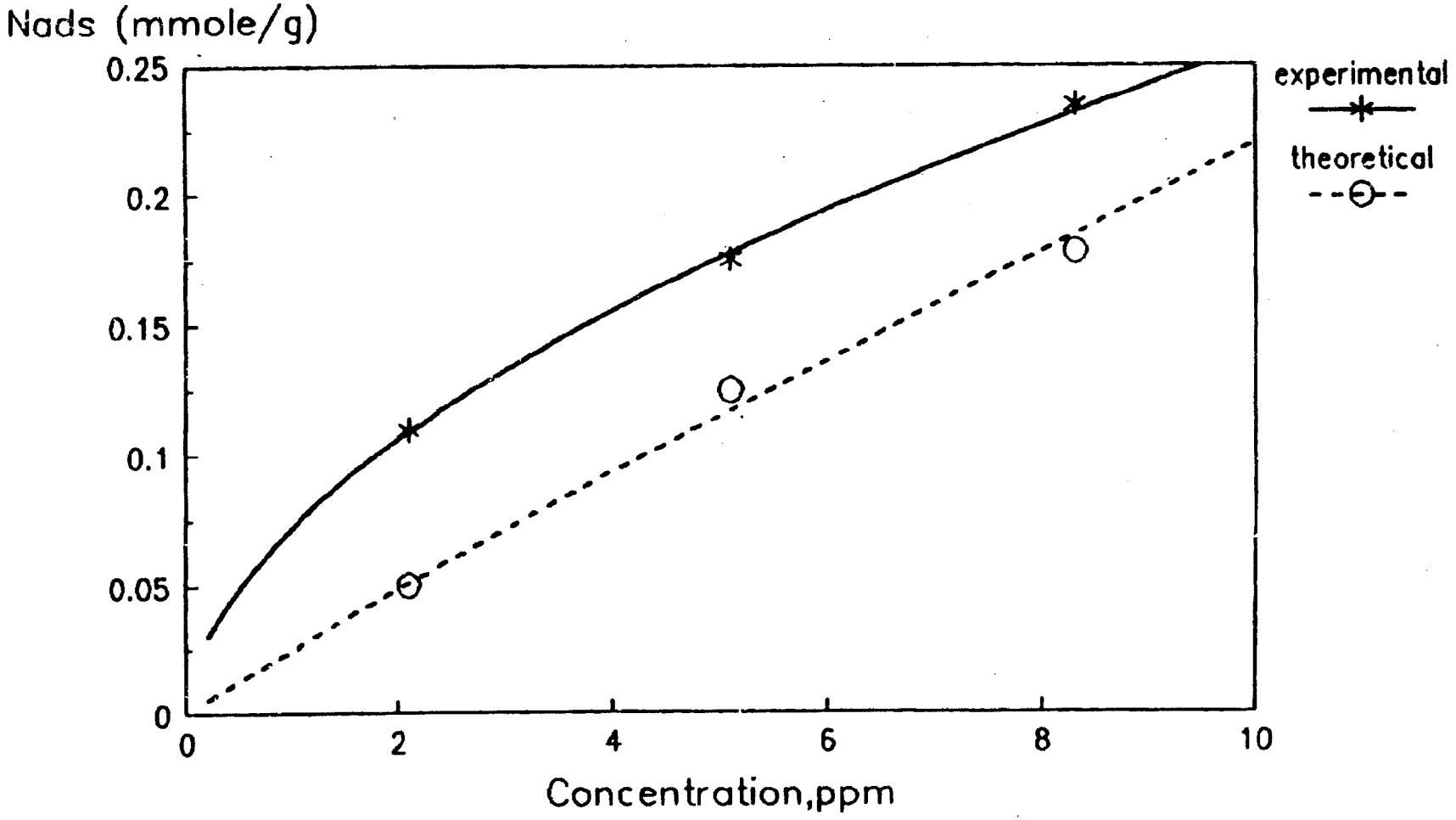

Adsorbent Selection for $Fe(CO)_5$ Adsorption

Of the adsorbents screened for $Fe(CO)_5$ removal, BPL carbon and H-Y zeolite are both useful adsorbents. At 90 psig (85% CO_2/14% CO/1% N_2) and 5 ppm, the capacities of BPL carbon and H-Y zeolite are 0.62 and 0.18 mmole/g, respectively. Thus, activated carbon has more than three times the capacity of zeolite. However, zeolite has a number of advantages over carbon. First, regeneration experiments indicate that the capacity of activated carbon is reduced on thermal cycling, which is not the case for zeolite. Second, zeolite has a 40% larger bulk density than carbon. Finally, thermal regeneration of $Fe(CO)_5$ laden adsorbents may produce a pyrophoric material. This may prove to be more of a problem with carbonaceous adsorbents than with inorganic ones.

Adsorption of $Ni(CO)_4$

Adsorbents Screened

Due to the carcinogenic nature of $Ni(CO)_4$, the total number of experiments done with this adsorbate was kept to a minimum. Based on the results obtained with $Fe(CO)_5$, adsorption isotherms were measured for $Ni(CO)_4$ with BPL carbon and H-Y zeolite only.

Figure 15 shows $Ni(CO)_4$ adsorption isotherms on BPL carbon and H-Y zeolite at 75°F from 40 psig carrier (95% N_2, 5% CO). The capacities at an equilibrium concentration of 1 ppm $Ni(CO)_4$ for BPL and H-Y are 0.22 and 0.07 mmole/g, respectively. The corresponding values for $Fe(CO)_5$ adsorption

FIGURE 15

Ni(CO)4 Adsorption on BPL and H-Y

75 F and 40 psig

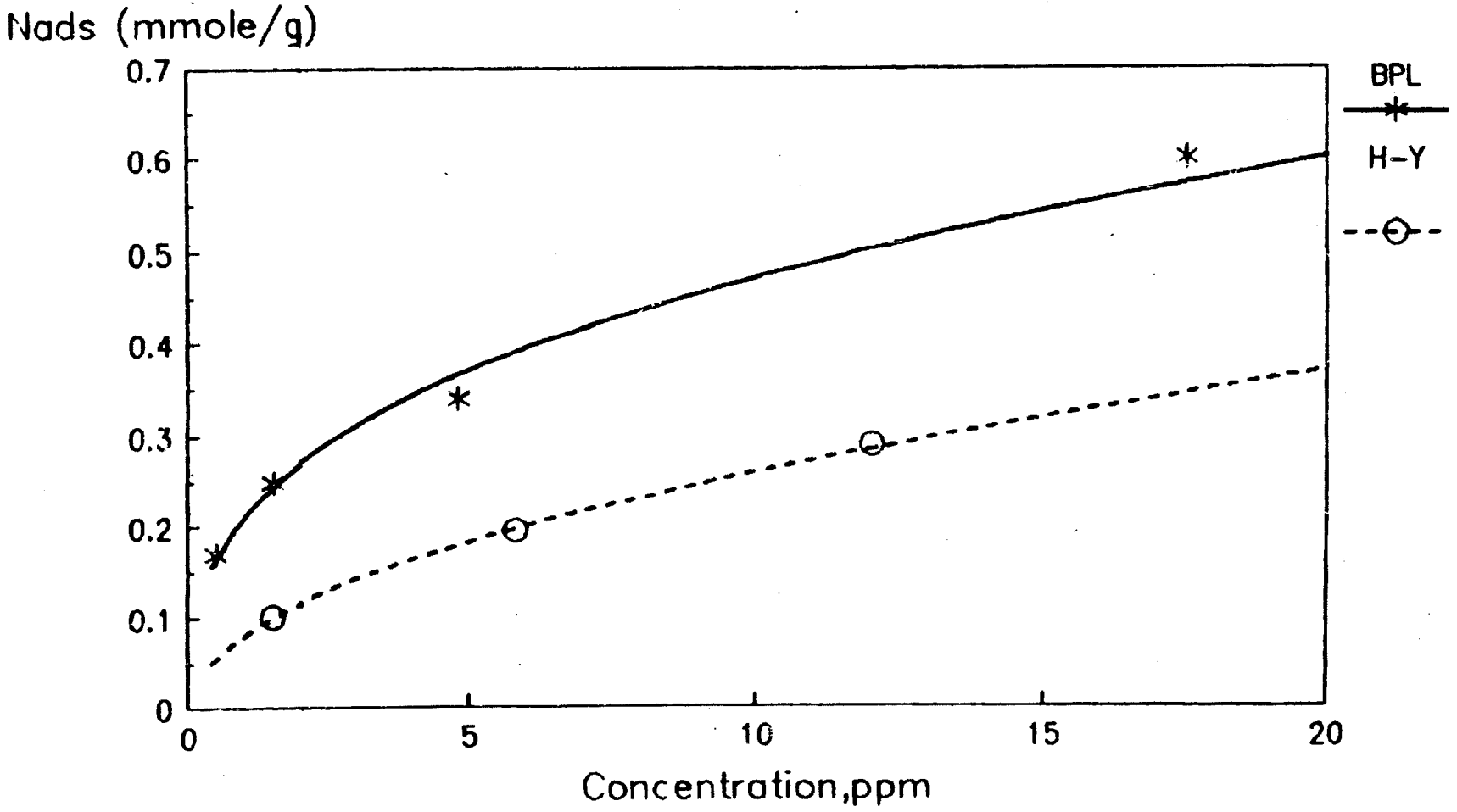

under the same conditions are 0.60 and 0.24 mmole/g. Thus, $Ni(CO)_4$ is adsorbed less strongly on these adsorbents than $Fe(CO)_5$ which is expected from the lower molar volume and higher saturation vapor pressure of $Ni(CO)_4$.

The Effect of Temperature on $Ni(CO)_4$ Adsorption

The effect of temperature on $Ni(CO)_4$ adsorption was investigated. Figure 16 shows $Ni(CO)_4$ adsorption isotherms on Linde H-Y from 40 psig carrier at 75 and 100°F. Figure 16 also gives the apparent heat of $Ni(CO)_4$ adsorption as a function of surface coverage. As was the case with $Fe(CO)_5$ adsorption, the magnitude of the heat of adsorption is large. At low surface coverage (0.05 mmole/g), the calculated heat of adsorption indicates a strong temperature dependence of $Ni(CO)_4$ adsorption. For example, the $Ni(CO)_4$ capacities at 1 ppm are 0.022 and 0.070 mmole/g at 100 and 75°F, respectively. Thus, the extent of $Ni(CO)_4$ adsorption can be largely affected by changing the adsorption temperature.

The effect of adsorption temperature on $Ni(CO)_4$ adsorption on BPL carbon was also investigated (Figure 17). As in all previous cases, the heat of adsorption is high and the decrease in heat as a function of surface coverage indicates adsorbent heterogeneity. Clearly, reducing adsorption temperature provides an effective means of enhancing the adsorptive capacity of adsorbents for carbonyls.

FIGURE 16

Effect of Temperature on Ni(CO)4 Adsorption

40 psig on H-Y

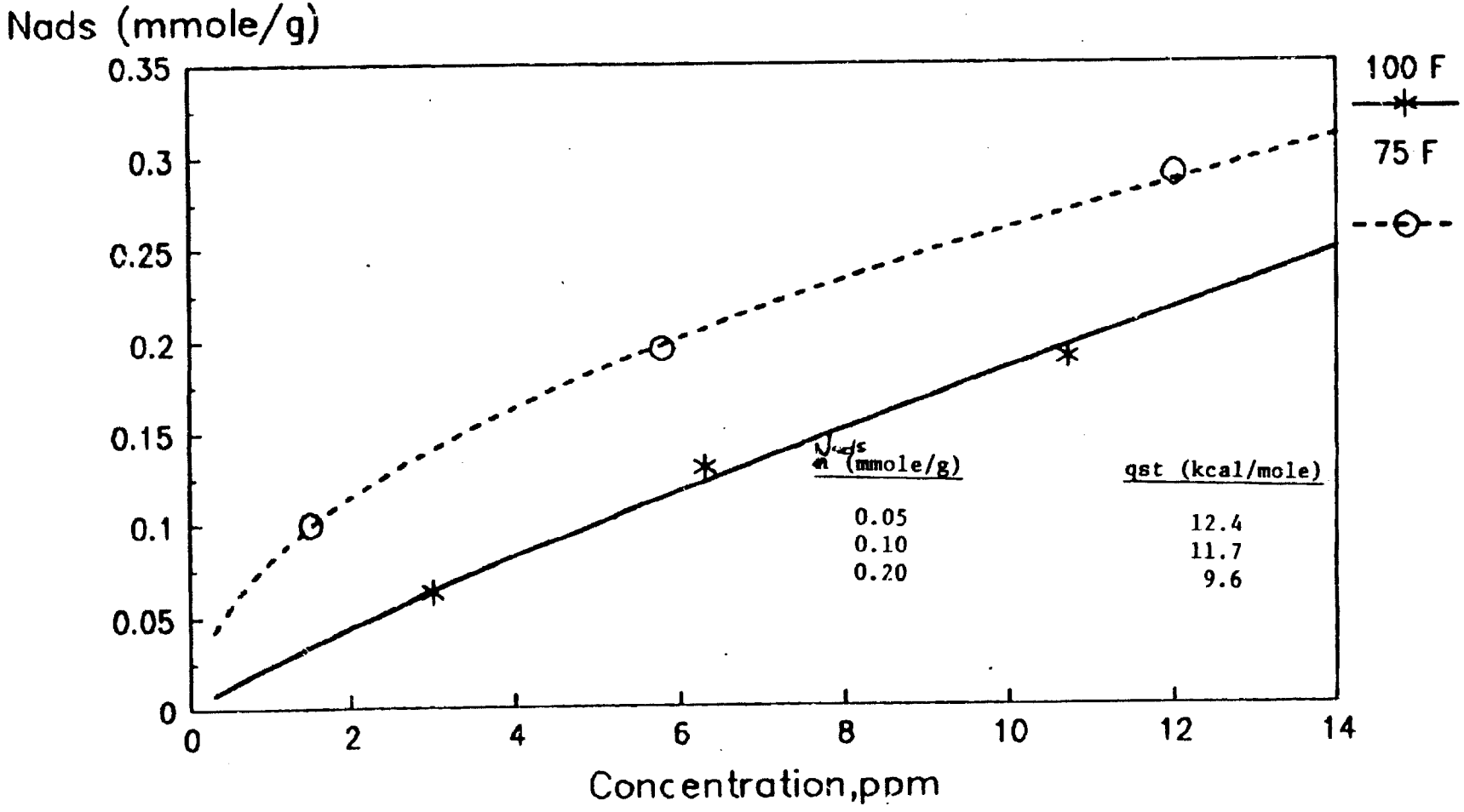

FIGURE 17

Effect of Temperature on Ni(CO)4 Adsorption
40 psig on BPL

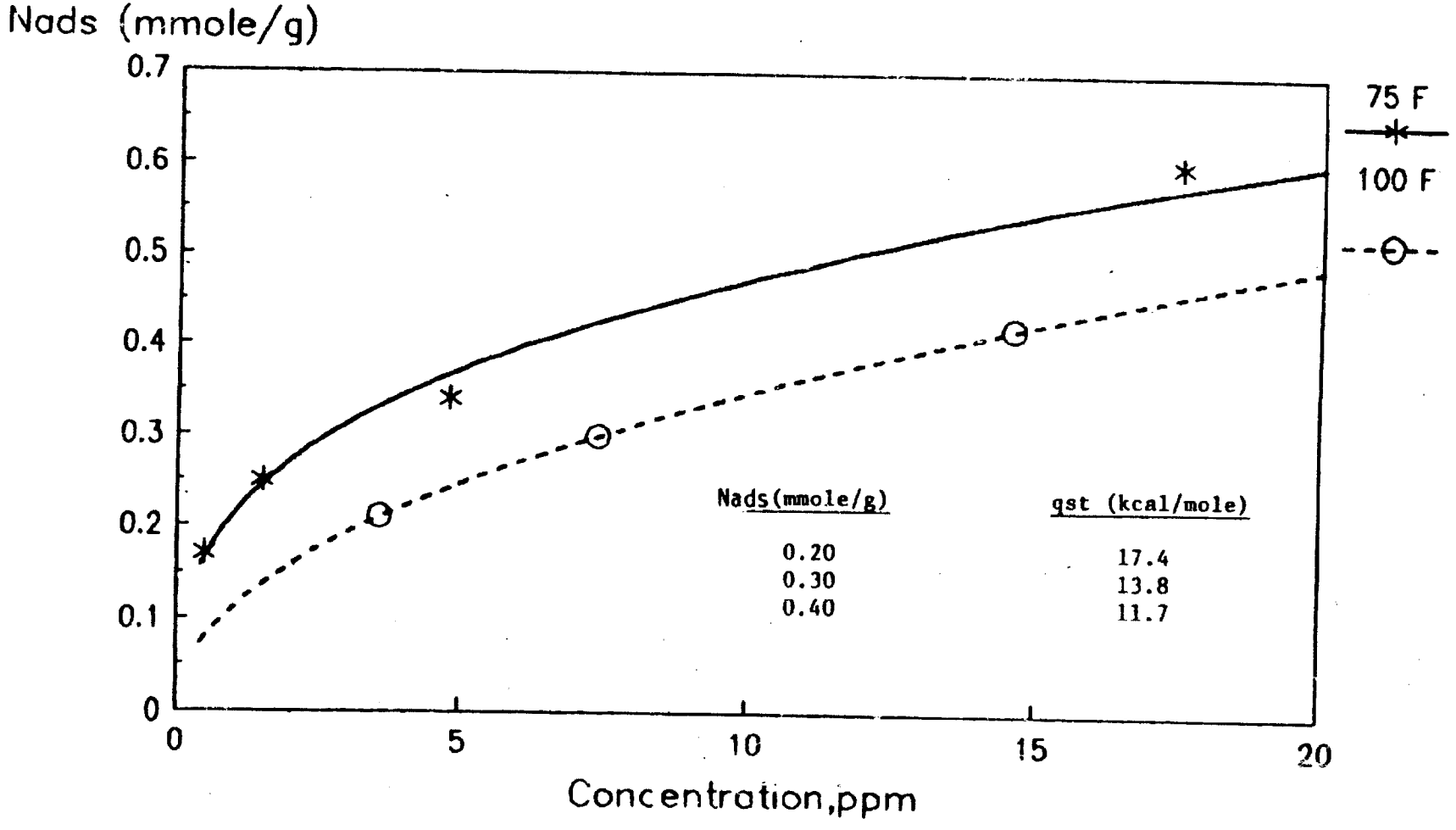

Effect of Carrier Gas Pressure on $Ni(CO)_4$ Adsorption

Figure 18 shows the effect of carrier gas pressure on the adsorption of $Ni(CO)_4$ on BPL carbon. As was the case with $Fe(CO)_5$ adsorption, higher carrier gas pressures decrease adsorption of the trace impurity. At 1 ppm $Ni(CO)_4$, the adsorption capacity of BPL carbon decreases from 0.20 to 0.05 mmole/g as the carrier gas pressure increases from 40 to 90 psig. This diminution is greater than that noted with $Fe(CO)_5$. This is to be expected since the effect of carrier gas pressure increases as the capacity for the trace impurity decreases. Thus $Fe(CO)_5$, which is adsorbed more strongly than $Ni(CO)_4$, is less affected by the carrier gas pressure.

Effect of Thermal Regeneration Studies on $Ni(CO)_4$ Adsorption

Figure 19 shows $Ni(CO)_4$ adsorption isotherms on BPL carbon at 75°F and 40 psig carrier (73% CO_2/26% N_2/1% CO) following three successive adsorption/regeneration cycles. Regeneration was carried out in N_2 at 250°F. As opposed to the $Fe(CO)_5$ adsorption/regeneration case, the $Ni(CO)_4$ capacity remains intact following these adsorption regeneration cycles. This is most probably due to the smaller capacity for $Ni(CO)_4$ than for $Fe(CO)_5$ demonstrated by BPL carbon.

Adsorbent Selection for $Ni(CO)_4$ Removal

The preferred adsorbent for $Ni(CO)_4$ removal is BPL activated carbon. The material demonstrates the highest $Ni(CO)_4$ adsorption capacity and is

FIGURE 18

Effect of Gas Pressure on Ni(CO)4 Adsorption

75 F on BPL

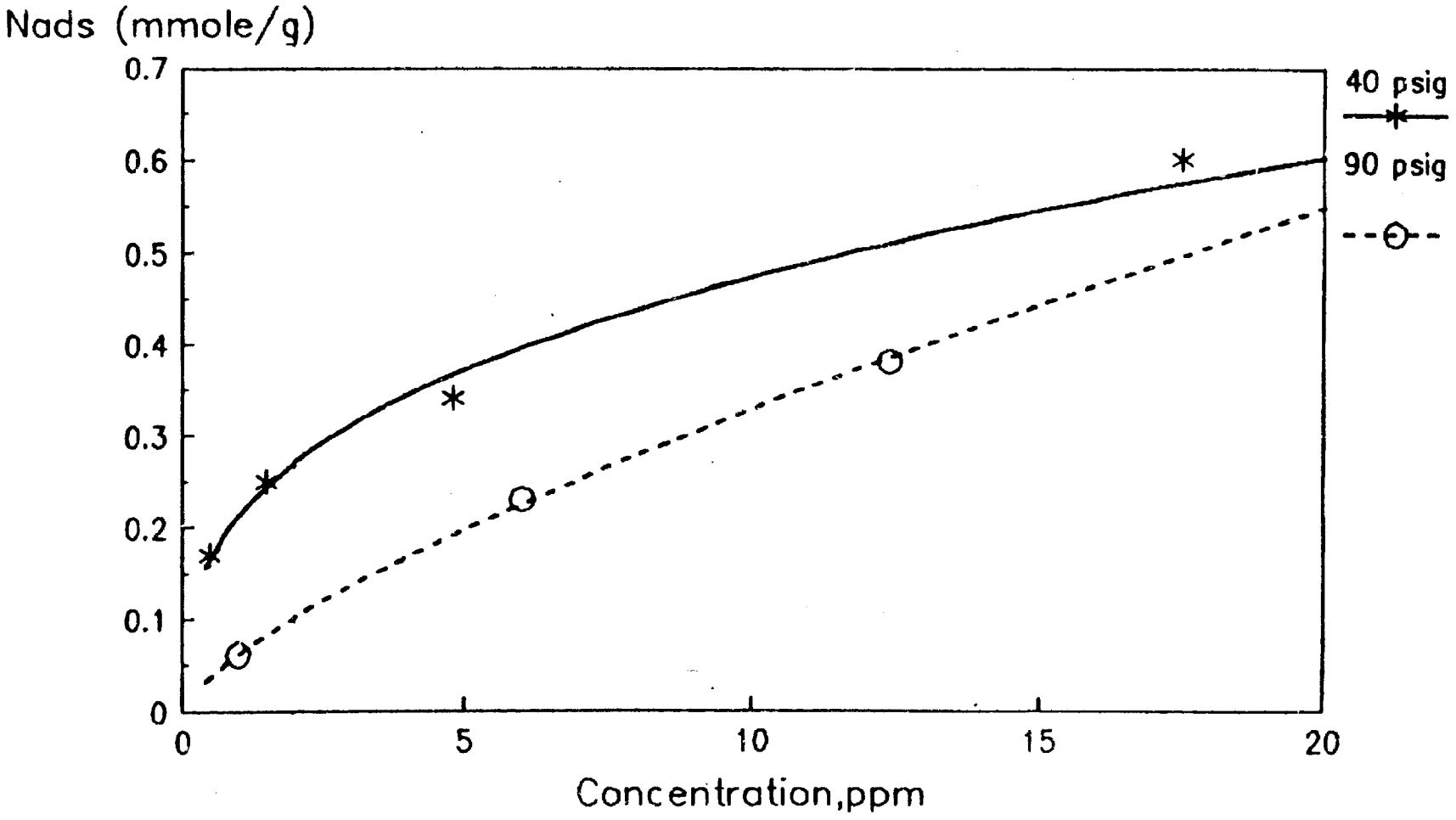

FIGURE 19

Effect of Regeneration on Ni(CO)4 Capacity

75 F and 40 psig on BPL

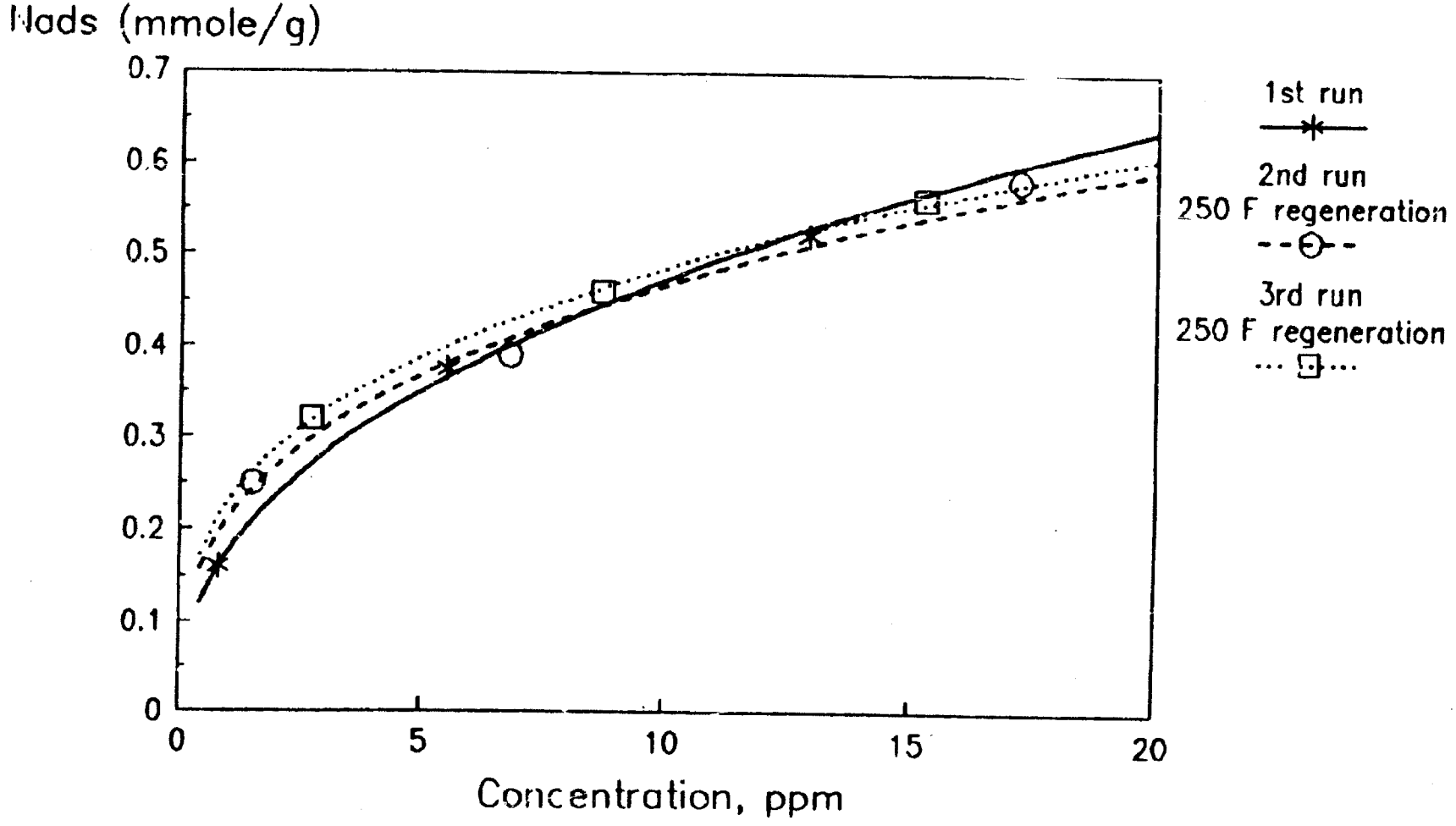

regenerable in N_2 at 250°F so that it should operate well in a conventional TSA system.

Adsorption of COS

Adsorbent Screening

Initial screening of adsorbents for COS removal was carried out by measuring adsorption isotherms at 75°F from 90 psig carrier gas (85% CO_2, 14% N_2, 1% CO). The adsorbents screened included a zeolite (Linde H-Y), an activated carbon (BPL carbon), a metal oxide promoted alumina (Alcoa Selexsorb COS), a metal oxide promoted zinc oxide (UCI-C125-1-01), an iron oxide impregnated activated carbon (Barneby-Cheney type CJ), a sodium oxide impregnated carbon (10% Na_2O on BPL), a copper oxide/chromium oxide impregnated carbon (Calgon type FCA), and a spent methanol catalyst (ICI EPJ-19).

The results of adsorbent screening are shown in Figure 20. First, only type FCA carbon shows appreciable adsorption capacity for COS. The adsorption capacities of H-Y and BPL carbon at an equilibrium concentration of 10 ppm are $\sim 2 \times 10^{-3}$ mmole/g. Clearly, this capacity is quite low. In addition, the capacities of sodium oxide and iron oxide impregnated carbon as well as promoted alumina and zinc oxide are lower than that for zeolite and activate carbon. Second, spent MeOH catalyst, EPJ-19, demonstrates the second highes COS capacity. Thus, those adsorbents screened with high COS capacity, EPJ-1 and FCA, both contain copper.

FIGURE 20

COS Adsorption on Various Adsorbents
75 F and 90 psig

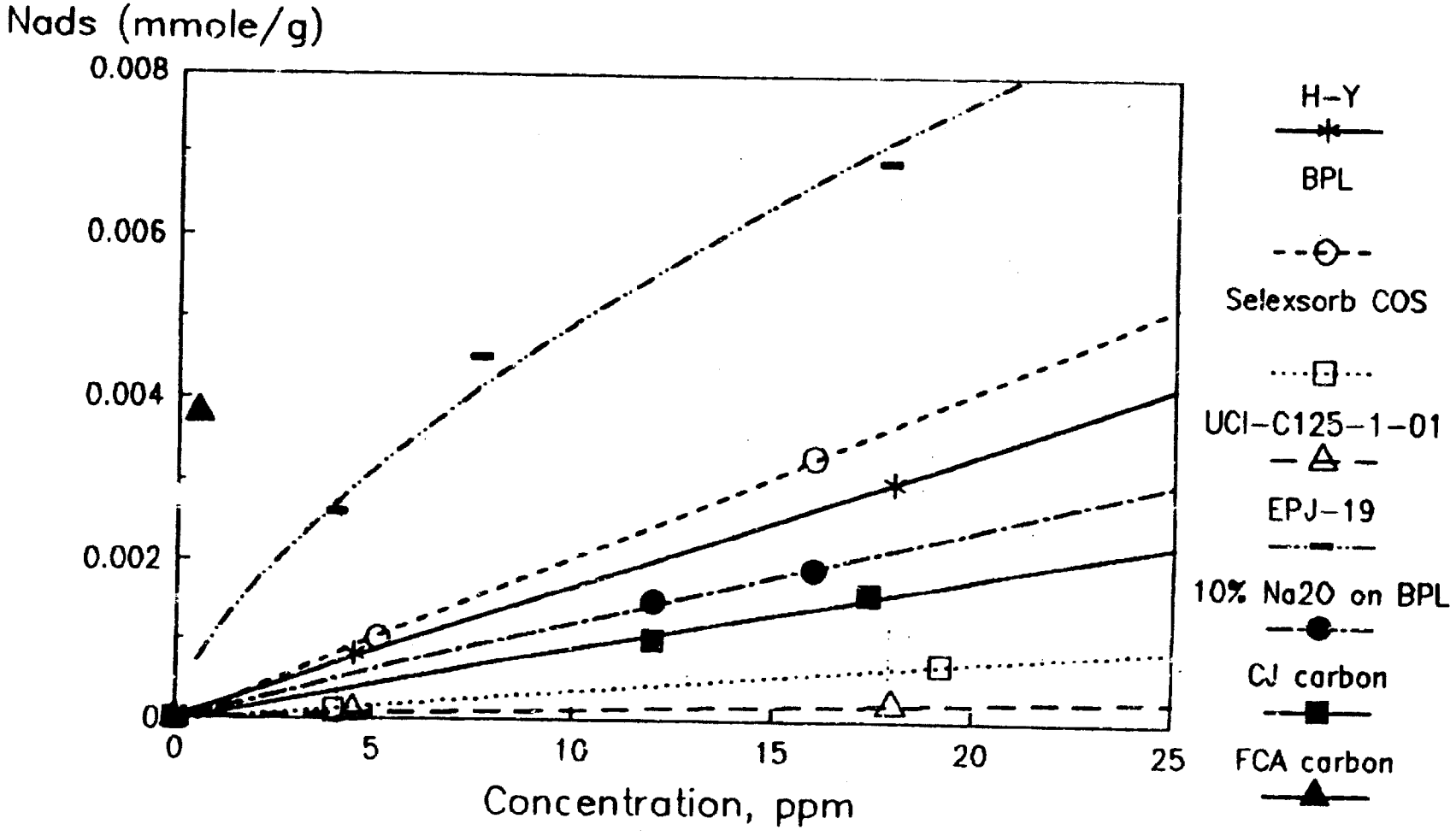

Effect of Regeneration on COS Adsorption on FCA Carbon

Since FCA carbon displayed the highest COS capacity of all adsorbents screened, the ability to regenerate the adsorbent was investigated. Figure 21 shows successive COS adsorption isotherms at 75°F and 90 psig carrier (85% CO_2, 14% CO, 1% N_2) on FCA carbon following various regeneration conditions. A freshly regenerated FCA sample showed a COS capacity of 0.067 mmole/g at an equilibrium concentration of 10 ppm. The "spent" adsorbent was then regenerated in N_2 at 250°F for 16 hours. The resulting COS capacity at 10 ppm dropped to 0.028 mmole/g indicating that this regeneration condition did not totally recover the COS capacity. To test the effect of regeneration gas, the sample was then regenerated for 16 hours at 250°F in CO_2. Again, the COS capacity was less than the original, indicating that the regeneration gas had no effect on the ability to regenerate the COS capacity. Finally, the effect of regeneration temperature was investigated and the sample was regenerated in N_2 at 500°F in N_2 for 16 hours. This treatment recovered the initial COS capacity. Subsequently, the adsorbent was regenerated again at 500°F in N_2 to ensure that the capacity remains intact following an adsorption/regeneration cycle at 500°F. After this second regeneration at 500°F, the COS capacity remained constant. Thus, type FCA carbon is a reversible COS adsorbent with regeneration at 500°F in N_2.

Effect of Temperature on COS Adsorption

The adsorption of COS on fresh type FCA carbon was carried out at 100°F so that the apparent isosteric heat of COS adsorption could be calculated.

FIGURE 21

Effect of Regeneration on COS Capacity

75 F and 90 psig on FCA carbon

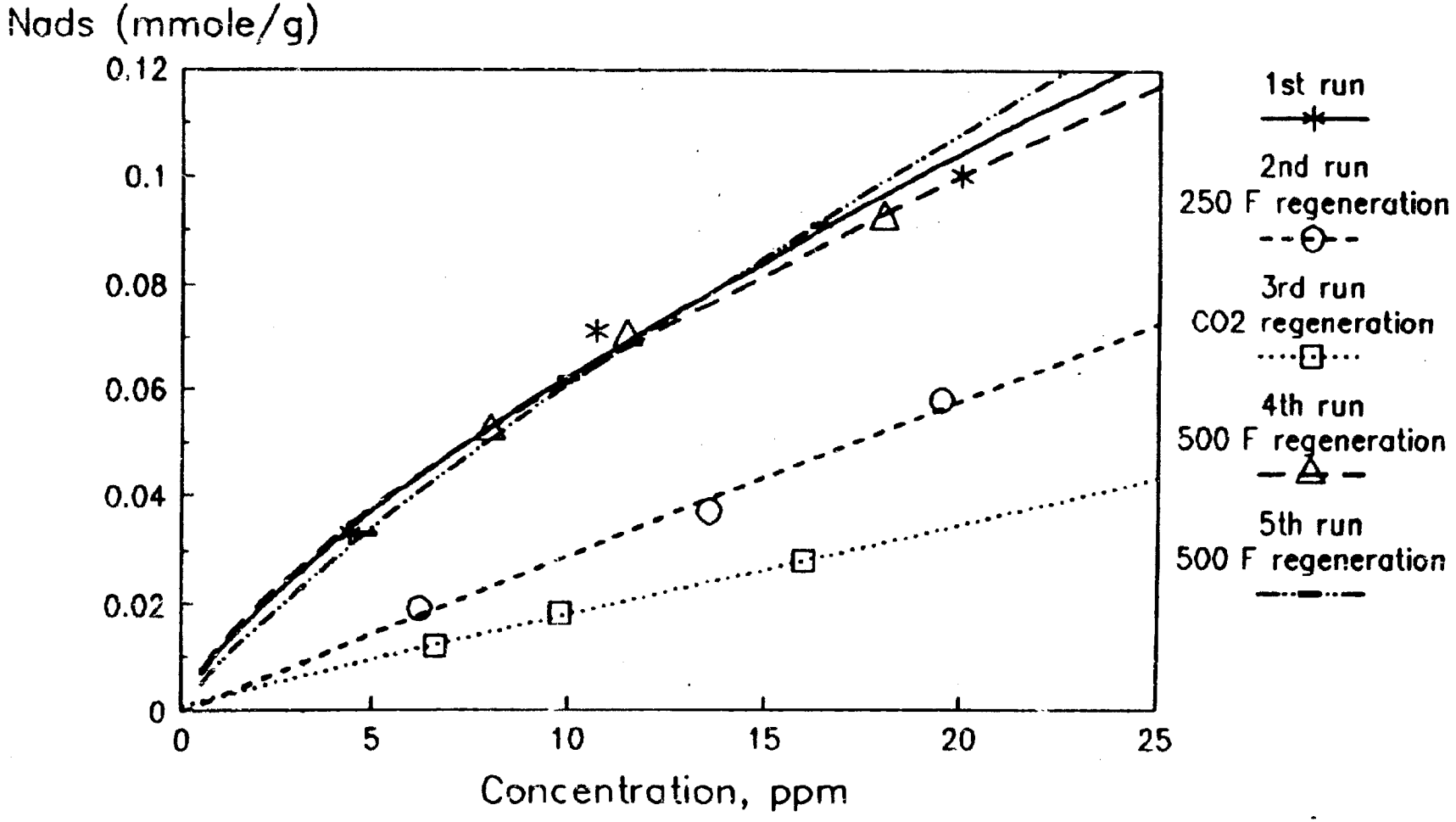

Figure 22 shows trace COS isotherms at 75 and 100°F. Also shown is the apparent heat of COS adsorption as a function of surface coverage. The apparent heat of adsorption at low surface coverage (0.01 mmole/g) is 13.1 kcal/mole; this value drops to 10.9 kcal/mole at 0.04 mmole/g indicating some adsorbent heterogenity. Furthermore, this relatively high heat of adsorption suggests that adsorption capacity can be significantly enhanced by reducing the adsorption temperature.

Adsorbent Selection for COS Removal

Of all the adsorbents screened, the preferred adsorbent for COS removal by adsorption at ambient temperatures is Calgon type FCA carbon. This adsorbent can be used in a regenerable temperature swing adsorption system with regeneration occurring at 500°F.

Adsorption of H_2S

Adsorbent Screening

Initial screening of adsorbents for H_2S removal was done by measuring trace H_2S adsorption isotherms at 75°F from 90 psig carrier gas (85% CO_2, 14% CO, 1% N_2). The adsorbents screened (as shown in Table 3) included two zeolites, Linde H-Y and Laporte CaX; BPL activated carbon; three impregnated active carbons, Calgon type FCA, desulf-B, and 10% (wt) MgO loaded BPL; two spent MeOH catalysts, EPJ-19 and BASF S3-85; and a promoted zinc oxide, Haldor-Topsoe, HTZ-4.